Engineering Fracture Mechanics 186 (2017) 331–346

Contents lists available at ScienceDirect

Engineering Fracture Mechanics

journal homepage: www.elsevier.com/locate/engfracmech

Stress intensity factor solutions for fretting fatigue using stress gradient factor

Marcelo Avelar Antunes [a], Cosme Roberto Moreira da Silva [a], Eduardo Martins Fontes do Rêgo [b], Antonio Carlos de Oliveira Miranda [c,*]

[a] Department of Mechanical Engineering, University of Brasília, SG-9 Building, Darcy Ribeiro Campus, DF 70.910-900, Brazil
[b] Department of Structure, Federal University of Piauí, Technology Center, Ministro Petrônio Portella University Campus, PI 64049-550, Brazil
[c] Department of Civil and Environmental Engineering, University of Brasília, SG-12 Building, Darcy Ribeiro Campus, DF 70.910-900, Brazil

ARTICLE INFO

Article history:
Received 21 August 2017
Received in revised form 26 October 2017
Accepted 27 October 2017
Available online 28 October 2017

Keywords:
Fretting fatigue
Weight function
Stress intensity factor
Stress gradient factor

ABSTRACT

This paper presents stress intensity factor (SIF) solutions for fretting fatigue conditions by including a stress gradient factor (SGF) to correct the classic geometry factor for tension semi-infinite strip (TSIS) specimen. This gradient factor considers the stress gradient due to the pressure of the pad on the surface of the specimen, which creates a high concentration of stresses around the contact of the bodies. To obtain these solutions, 2D finite element model simulations were performed varying important fretting parameters, namely: coefficient of friction, bulk stress intensity, pad radius and material. All configurations respected a partial slip contact condition and the results obtained show agreement with the ones obtained analytically. Weight functions were used to obtain stress intensity factors under mode I, then to compute the SGF, which were fit into equations with a unique structure, varying only coefficients. To consider real problems, a 3D correction factor was introduced. The final SGF presented a general form to compute SIF under fretting conditions when applied in suggested methods, such as: Strain-based Fracture Mechanics, Theory of Critical Distances (TCD) and Stress Gradient.

1. Introduction

The fretting fatigue phenomenon occurs whenever relative displacements are found between two different contact surfaces submitted to oscillatory load. Because its occurrence reduces the lives of components greatly, understanding how it works is of great importance. It was pointed out by Madge et al. [1] that the most damaging situation in fretting occurs under a mix of gross and partial slip regime. The latter is critical because it will always reduce the specimen's life, since it raises the slip amplitude between the surfaces. The same doesn't always hold true for the former, which is also much related to wear. The partial slip regime occurs whenever $Q < \mu P$ [2] (where Q is the tangential load on the contact, μ is the coefficient of friction and P is the applied normal load) and the analytical contact solutions for this condition based on the contact theory proposed by Hertz were demonstrated by [3] for cylindrical pads. Also, there is good agreement in the literature [1] that among all properties involved in fretting fatigue, the relative slip amplitude, the contact pressure and the friction coefficient between the two surfaces are the most important.

* Corresponding author.
E-mail addresses: marcelo.avelar.antunes@gmail.com (M.A. Antunes), cosmeroberto@unb.br (C.R.M. da Silva), e_eduardofontes@ufpi.edu.br (E.M.F. do Rêgo), acmiranda@unb.br (A.C. de Oliveira Miranda).

https://doi.org/10.1016/j.engfracmech.2017.10.031
0013-7944/

In order to verify the importance of fretting fatigue analysis over time, a bibliometric analysis was performed. The topic search "Fretting" was created in the ISI Web of Science database for the period of 1970 until 2017 (on September, the 24th) and it was observed that the production of papers containing the term "Fretting" has been overall increasing considerably. However, the same holds true for many engineering topics, as well as to numerical methods. For that reason, as displayed in Fig. 1, the number of articles containing the keyword "Fretting" was compared to the number of articles containing the keywords "Finite element method" (FEM) and "Fatigue". Note that the number of fretting articles produced maintains the same ratio when compared to "Fatigue" and "FEM" since 2000. Since the latter topics are much broader than the former and display a significant increase of production over the years, it can be inferred that there has been a constant interest by the scientific community of studying the fretting phenomenon.

Many numerical models were already proposed in order to properly emulate the rather complex fretting phenomenon. Despite many satisfactory results being found as in [4,5], these studies usually address specific conditions that require mesh remodeling if the initial set up is changed. Another difficulty for properly modeling the phenomenon is that certain properties may vary greatly during simulation according to material properties, loading and boundary conditions. This leads sometimes to quite complex models that may be of difficult practical broader use.

Multiaxial fatigue models were often used to determine crack nucleation direction [6–10], usually associated with a propagation model. Not all articles accounted for tridimensional effects on crack propagation. Some authors created 3-D FEM or Extended finite element method (X-FEM) models to directly establish tri-dimensional crack propagation [2,5,9,11,12], with a few proposing simplifications using both 2-D and 3-D analysis [2,5,12] with the goal of reducing computational costs. On the other hand, [11] simplify it by using an established correction factor.

Furthering the analysis, it was perceived that in order to avoid mesh remodeling for each configuration, as for load changes or crack growth, some authors made use of the X-FEM [5,11,13], while others [4,6,14–16] used Weight Functions (WF) associated with Stress Intensity Factors (SIF). To address plasticity, many studies used the in-built function of the software ABAQUS or sub-modeling techniques that enabled the use of the elastoplastic properties of materials [7,8,12,17].

Aiming to compute SIF under fretting conditions, some researchers have proposed analytical SIF solutions. Hills & Nowell [18] presented many different approaches in order to calculate the SIF, e.g. a general solution based on Green's function together with the Bueckener superposition principle for an infinite body. However, these solutions are based on linear contact analysis and they do not consider real boundary conditions for real situations. Hills & Comninou [19] studied SIF for various crack lengths, coefficients of friction and applied load ratios. In their study, a constant normal pressure and a sinusoidal shear load were applied on the contact surface, in which geometry and loading conditions were approximations of the classical fretting problem. Giummarra & Brockenbrough [20] estimated SIF by linear equations for a crack in the edge of a half plane subjected to normal, tangential and fatigue loading. Other works, as described by Ciavarella & Berto [21], study analytical SIF as an analogy with a notch, the so called "Crack Like Notch Analogue" (CLNA) model. The main problem with these described analytical SIF solutions are the lack of the non-linear behavior of contact, which changes all behavior of stresses around the crack tip. However, they serve as parameters to more complex analyses.

Based on the extensive research of previous works, the authors acknowledge that there are no general expressions such as found in the Handbook published by Tada et al. [22], in which the SIF is expressed in term of geometry factors f(a/w), for SIF of cracks originated from the contact of two bodies under fretting condition. Therefore, it is possible to anticipate that the main contribution of this work is to provide a more general SIF solution, expressed in terms of a stress gradient factor, for fretting analysis considering different geometries, materials and loadings, hence filling the aforementioned gap.

The structure of this article is divided into 7 sections. In the second, the main idea of the paper is explained, followed by the elucidation of how the numerical SIF were obtained. Section four details the created numerical models, as well as their validation. It also explains thoroughly all the considerations taken into account so that the results could finally be presented

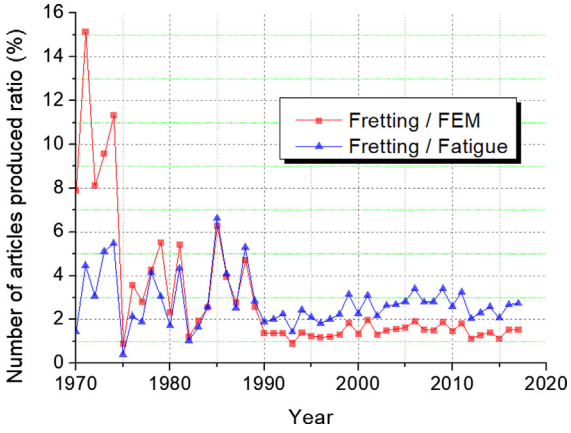

Fig. 1. Evolution of fretting-related articles production in comparison to the FEM and fatigue topics from 1970 until October-2017.

and discussed in Section 5. Finally, the potential and usefulness of the concept proposed in this work is demonstrated in Section 6, with the conclusion being presented afterwards.

2. Main concept

The concept herein proposed is based on the idea of Topper & El Haddad [23], which presented the definition of elastic stress concentration factor (ESCF), K_p, to predict fatigue lives of notched specimen and weld toes. K_p accounts for the increase in crack tip stress due to a notch or a flaw in a notch. Its equation is given by

$$K_p = \frac{K}{\sigma\sqrt{\pi a} f(a/w)} \tag{1}$$

where K is the stress intensity factor, σ is the nominal stress, a is the crack length, and $f(a/w)$ is the geometry factor that accounts for crack shape and finite specimen size. Topper & El Haddad [23] replaced the theoretical stress intensity factor, K_t, by K_p to compute strain range deformation in cyclic stress-strain equations together with Neuber's rule. In this case, the crack growth was dictated by a non-uniform stress/strain field and required the use of the ESCF instead of the theoretical (classical) stress concentration factor (SCF), which is limited to the surface of notch roots. Topper and co-authors used the term ESCF in other papers [24,25].

In 2011, Gharemani &Walbridge [26] used the same concept proposed by [23] but introduced the term strain-based fracture mechanics (SBFM) for the method presented by Topper & El Haddad. They applied SBFM to study fatigue of material in penned highway bridge welds under variable amplitude loading conditions. However, K_p is mentioned as stress concentration factor, creating confusion with theoretical (classical) SCF. Gharemani et al. [27] followed the previous work to propose a methodology for variable amplitude fatigue analysis in welds using again SBFM. In that work, K_p is referenced as modified stress concentration factor (MSCF) and the nomenclature was changed to k_p.

In the opinion of the authors of this work, the terms ESCF, SCF or MSCF are not adequate to represent the equation (1), because it is a ratio between two stress intensity factors. In fact, Eq. (1) can be rewritten as:

$$K = \sigma\sqrt{\pi a} f\left(\frac{a}{w}\right) \cdot K_p = K_{ref} \cdot K_p \tag{2}$$

where the SIF (K), of a desired geometry for analysis, is computed by K_{ref}, a stress intensity factor for a reference geometry, and K_p, which is a factor to correct the K_{ref}. As described previously, this factor was used in notched specimen and weld toes that create a stress gradient around the geometry of notch root.

The authors propose to modify the mentioned terms ESCF, SCF and MSCF to Stress Gradient Factor (SGF), $K_{gr}(a/w)$, because it modifies a SIF (reference) when a gradient stress is present in geometry specimen and it is much like the geometry factor $f(a/w)$. Fig. 2 visually represents the idea of $K_{gr}(a/w)$ for the fretting problem. This work intends to compute SIF in fretting condition, as shown in Fig. 2(a), by calculating the SIF of a tension semi-infinite strip (TSIS) specimen (Fig. 2(b)) and correcting it with a Stress Gradient Factor that takes into account the gradient stress produced by the pad pressure on the specimen. This is the main concept of this paper to compute SIF in fretting conditions.

After rewriting Eq. (2) to compute the SGF, the following equation can be used to compute SIF in fretting conditions:

$$K_I = K_{I(ref)} \cdot K_{gr}(a/w) \rightarrow K_{gr}(a/w) = \frac{K_I}{K_{I(ref)}} \tag{3}$$

where K_I is computed using the approach described in Section 3 and the TSIS specimen is used to compute $K_{I(ref)}$. The geometry factor $f(a/w)$ for the TSIS specimen is given by [21]:

$$f(a/w) = \left\{0.857 + 0.265\left[\frac{a}{w} + \left(1 - \frac{a}{w}\right)^{5.5}\right]\right\} / \left(1 - \frac{a}{w}\right)^{1.5} \tag{4}$$

Now, it is possible to present the differences among K_I, K_t and K_{gr} as shown in Table 1, avoiding any problem with nomenclature and definition.

3. Numerical SIF

A study of historical and state-of-the-art Computational Fracture Mechanics techniques as well as a taxonomic research of the different cracking processes representations was presented by Ingraffea [28], dividing such approaches into geometrical and non-geometrical. Two major methods are used for the former: Constrained (prescribed, analytical geometry and known solutions methods) and Arbitrary (meshfree, adaptive FEM/BEM, lattice, particle and atomistic methods). Two other major methods are used for the latter: Constitutive (smeared crack, element extinction and computational cell methods) and Kinematic (Enriched element method and XFEM/GFEM) methods.

The Weight Function method [29,30] is a Known Solution Method [28] and was herein employed to calculate stress intensity factors (SIF). It was successfully used for such purpose before [31–33] and its main advantage is that it allows the loading analysis to be performed apart from the geometry. For a determined cracked geometry, any applied load to the body in ques-

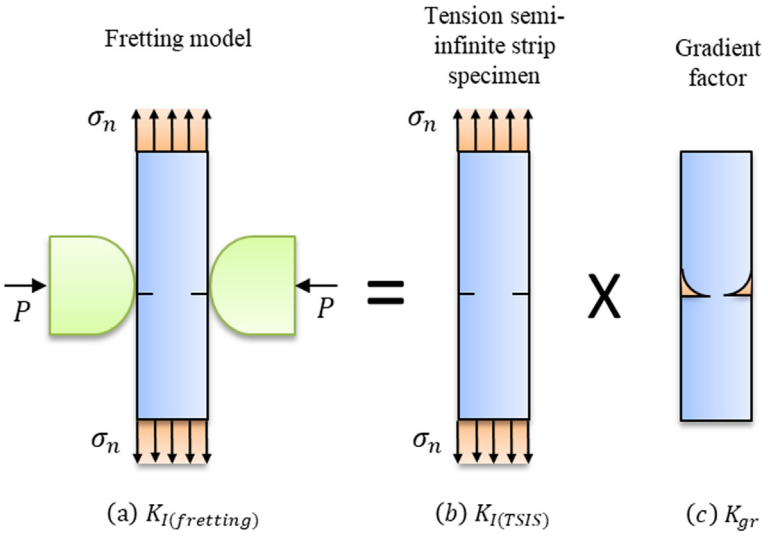

Fig. 2. General concept of the use of SGF.

Table 1
Main characteristics of K_I, K_t and K_{gr}.

	K_I	K_t	$K_{gr}(a/w)$
Definition	Stress Intensity Factor (Mode I)	Stress Concentration Factor	Stress Gradient Factor
Equation	$\sigma\sqrt{\pi a}\cdot f(a/w)$	σ_{max}/σ	$\frac{K_I}{K_{I(ref)}}$
Applicability	da/dN, Crack propagation	εN, SN, Crack initiation	Short Crack initiation and propagation

tion will have its effects computed by the same known weight function.According to Glinka & Reinhardt [34], the following tasks are necessary prior to obtaining the SIF using the weight function method:

- Computation of the stress distribution along a defined plane using linear elastic analysis;
- Application of the aforementioned stress distributions to the crack surface;
- Choice of the appropriate generic weight function;
- Integration of the product of the stress function and the weight function over the crack length or the crack surface.

The SIF is then obtained by integrating the product between the weight function $m(y,a)$ and the stress field of the uncracked body $\sigma(y)$ over the crack length a:

$$K_I = \int_0^a \sigma_x(y) m(y,a) dy \tag{5}$$

The values of $\sigma_x(y)$ are obtained through FEM by extracting the stress fields in a straight line from the maximal normal stress $\sigma_{x_{max}}$ as displayed in Fig. 3(a).

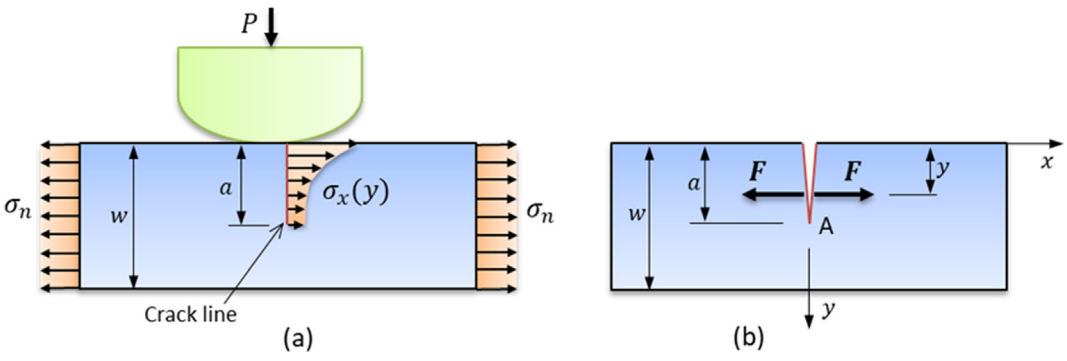

Fig. 3. Stress field extraction path used to compute K_I (a) and geometry configuration used for single edge crack (b).

The main advantage of using weight functions is that the stress fields of the uncracked body can be used to further computation of the Stress Gradient Factor (SGF), which excludes the necessity of mesh remodeling with crack growth.

A vast number of one-dimensional weight functions for different geometries were suggested by Tada et al. [22] in their handbook, each containing a different formula for every different crack geometry. Glinka & Shen [33] suggested an Eq. (6) that could be used for any crack geometry, in which only the different M_i parameters are modified accordingly. The crack geometry used in this study is illustrated in Fig. 3(b), where a is the crack length, w is the specimen width, F is the force, y is the distance between the specimen surface and the load F and K is determined at point A.

For the geometry represented in Fig. 3(b), the weight function $m(x,a)$ is given by:

$$m(y,a) = \frac{2F}{\sqrt{2\pi(a-y)}}\left[1 + M_1\left(1-\frac{y}{a}\right)^{1/2} + M_2\left(1-\frac{y}{a}\right)^{1} + M_3\left(1-\frac{y}{a}\right)^{3/2}\right] \tag{6}$$

where the M_i parameters are specific for each crack configuration. In this work, considering a single edge crack in a finite plate, the coefficients were borrowed from [35] and can be found in Appendix A.

4. Numerical model

This section demonstrates how to obtain the stress distribution in fretting geometry using the Finite Element Method in order to compute SIF by integrating this stress distribution and weight functions. At first, the materials, bulk stresses and boundary conditions were chosen to properly create a finite element model using ANSYS. The output simulations were compared to the analytical solution found in [3] and validated. The point on the specimen's top surface correspondent to the maximum normal stress was considered to display the most critical situation. Therefore, the stress fields under a straight line from that point were extracted to compute the SIF under mode I $K_{I(fretting)}$ [4,6,14–16]. The nature of such weight functions made it unnecessary to refresh stress fields as the crack progressed and $K_{I(fretting)}$ was finally used together with $K_{I(ref)}$ to calculate $K_{gr}(a/w)$.

First of all, it was necessary to choose the materials to be analysed. The materials chosen were steel, aluminum and titanium alloys. For each simulation, the pad and the specimen were set with the same material. This choice was based on their vast engineering use as components subjected to fretting fatigue [2,7,9,13,36,37]. Once the material properties were used as an input, it was necessary to determine the applied bulk stresses. Therefore, since the latter play a major role in fretting fatigue, discovering their relation to K_{gr} was of great interest. For that reason, simulations were produced for each material with bulk stresses of 100, 80 and 60 MPa.

The maximum bulk stresses that still respected the partial slip regime were estimated for all materials. The most critical value was then used for all materials in order to assure that all models would still be in partial slip regime for the defined configuration. This criterion was adopted so that further analysis containing different materials, such as verifying the influence of elastic properties in K_{gr} behavior would not be affected by the change of the bulk stresses themselves. Since the coefficient of friction (COF), μ, is also very relevant in fretting analyses, its behavior was also studied fixing all other previously mentioned parameters and correlating its changes to the ones observed for K_{gr}. The COF adopted were of 0.9, 0.75, 0.65 and 0.55, covering a great range of values present in the literature [2,7,9,13,36,37].

At last, for a specific case with steel, $\sigma_b = 100$ MPa and $\mu = 0.75$, pad radii were modified so that the effects on K_{gr} produced by such changes could be analysed. All other simulations used the standard value of 100 mm as the pad diameter.

36 models were created to cover all three materials in the first two cases (fixed bulk stress with mutable COF and vice versa) and 5 extra models were needed for the third case (pad radii variation), totalling 41 models.

The boundary conditions as well as the geometry of the 2D plane-strain models used in this study are illustrated in Fig. 4(a). It is noticeable that symmetrical properties in relation to Fig. 2(a) were used in order to reduce computational cost. The load Q was not applied to the surface directly but resulted as reaction of the bulk stress since the pad had its movement restricted in the x-direction and was in contact with the specimen.

The numerical simulation was divided into 3 sub-steps. At first, a small displacement of -5×10^{-4} mm was imposed to the pad against the specimen to assure that no rigid body motion would occur during the simulation and no singularity problem would happen. The second step consisted of removing such displacement and applying a vertical force P of -543 N to the pad top surface. In this step, the bulk stress was also introduced, starting from 0 and linearly ascending to its maximum at step 3.

A real fretting test takes thousands or millions of cycles of loading and only half a cycle was simulated herein. However, as the elastic condition is always satisfied in this model, the same stress fields are always computed for the same conditions, as it was verified later for 1.5 and 5.5 cycles with stress ratio R = 0 and agrees with previous studies [38–41].

The number of nodes, contact elements, solid elements and average time for each material simulation is presented in Table 2.

The coarse mesh was created by dividing 200 times both pad and specimen into quadratic elements. The contact half-width had already been calculated, which permitted the refinement of squared zones as depicted in Fig. 4(b). For the aluminum models, because the calculated contact size was larger, the inner square width was of 2 mm instead of 1.5. The contact zone mesh was then refined to squared 50 μm edge size elements in the external zone and refined to squared 5 μm edge

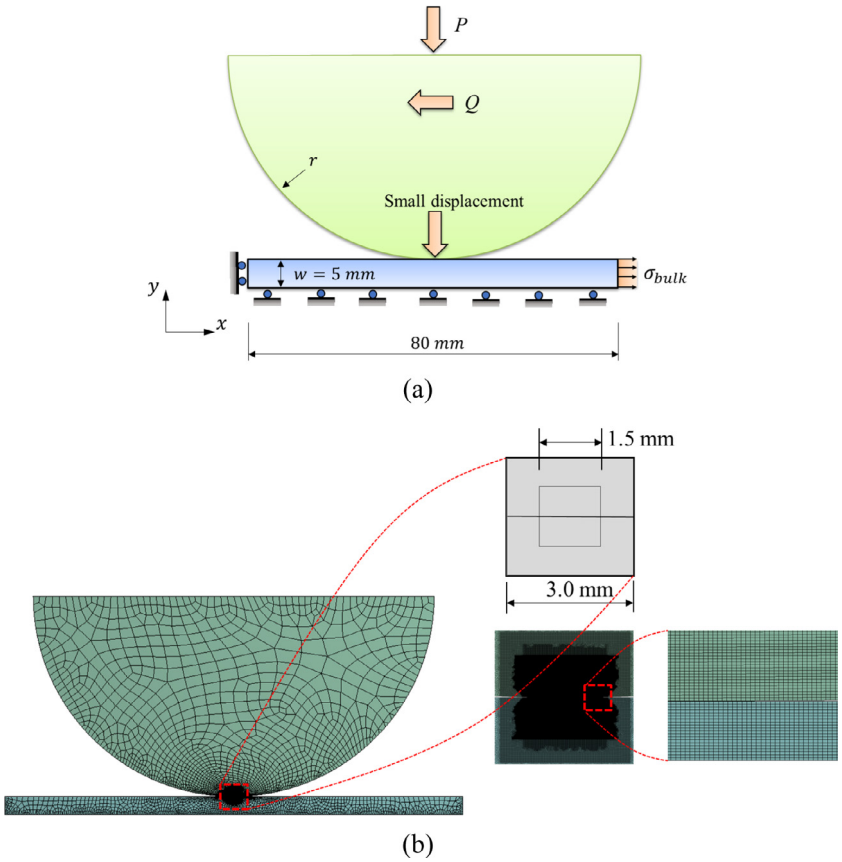

Fig. 4. (a) Numerical model boundary conditions and geometry and (b) Refined mesh for the whole model (left) and zoom of the contact mesh (right).

Table 2
Number of nodes, elements and time elapsed in simulations.

Material	Nodes	Contact elements	Solid elements	Total of Elements	Time elapsed (s)*
Steel	121069	1665	119923	121591	1488.6
Aluminum	151435	1683	150260	151946	2192.3
Titanium	121069	1665	119923	121591	1634.3

* Intel Core i5-6400 CPU @2.70 GHz with 32 GB RAM memory was used.

size elements in the external zone. These values were suggestions made by Talemi et al. [4], which used similar geometry and conditions. The final refined mesh for the model is shown in Fig. 4(b).

The numerical resolution was configured as static and the Newton-Raphson asymmetric method with sparse asymmetric matrix was used. The contact was defined by the Augmented Lagrange method with a ratio of 0.75.

Prior to further advancement of the model, it was necessary to evaluate the results, which was accomplished by comparing the numerical results to the ones obtained with the equations proposed in Nowell & Hills [3]. The materials properties used are shown in Table 3.

Since the contact half-width is much smaller than the specimen half-width, the infinite semi-plane assumption is valid.

For the aluminum simulation, it was found analytically a contact semi-width of 0.9118 mm, a stick zone semi-width of 0.36472 mm and a contact pressure, P_o, of 379.11 MPa when P = 543 N, Q = 296.25, μ = 0.65 and σ_{bulk} = 100 MPa. The comparison between theoretical and numerical results is shown in Fig. 5.

Table 3
Materials properties.

Material	Aluminum	Titanium	Steel
Modulus of Elasticity	74.1 GPa	127 GPa	200 GPa
Poisson's ratio	0.33	0.32	0.30

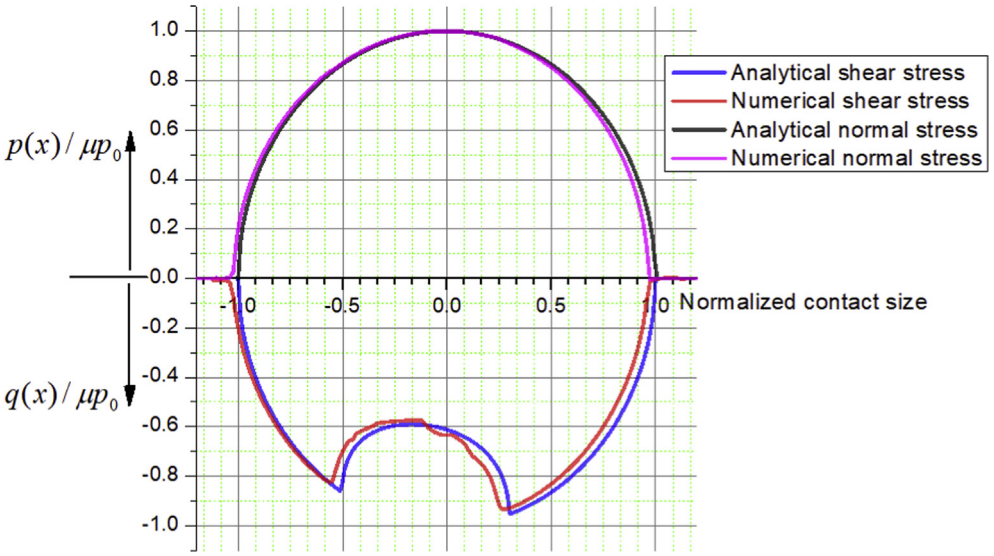

Fig. 5. Comparison between analytical and numerical results for aluminum alloy nominal stress (top) and shear stress (bottom).

The results obtained numerically show good agreement with the analytical solution. The error between the maximum contact pressure obtained analytically (379.11 MPa) and numerically (381.7 MPa) is less than 1%. Similar errors were found for all other materials. Whilst for normal stresses the numerical curves are practically coincident to the ones obtained analytically, it is possible to notice that shear stresses curves are not exactly coincident but close and display small disturbances within the contact adherence zone. This probably occurred because small bending moments emerged against the pad, as a reaction of the bulk stress and the horizontal restriction imposed and also because how the problem is formulated in ANSYS.

Under fretting conditions, the multiaxial stress fields are very complex and considerable efforts have been made by many researchers in order to understand the different behaviors of each stage of crack growth, as well as to predict crack growth direction. However, there is already much experimental evidence that cracks under the fretting regime are formed near the contact region, initially propagating in low angles in respect to the free surface and then kinking to higher angles, until a near perpendicular direction is reached. At this final stage, cracks continue to propagate almost linearly until failure.

In this work, the crack was considered to initiate at the point that achieves the maximum normal stress. The crack was then assumed to propagate linearly, perpendicular to the surface of the specimen. The path herein adopted is not realistic, as observed in multiple studies [4,5,42], because of its trajectory and because of the exact initiation location. For crack initiation and very small crack lengths, studies indicate that shear stress plays an important role [18]. Nonetheless, this straight crack path perpendicular to the free surface of the specimen has been used before satisfactorily in some fatigue researches [4,6,14–16,40].

To evaluate the effects on the mode I stress intensity factors (K_I) caused by such simplifications, finite element (FE) models were created in ANSYS with cracks containing the angles most frequently observed experimentally [5,39,40,43,44], as depicted in Fig. 6. The cracks in FE models were manually discretized in each desired position and the SIFs were evaluated using J-integral. It can be seen from Fig. 6 that most angles are between 10 and 22 degrees.

Fig. 7 displays the relative differences between K_I with perpendicular crack (0°) in relation to kinked cracks with 15° and 20° using FEM (J- integral) and WF. Furthermore, it compares the mode I SIF obtained with the two different methods for the straight crack path. The mode I SIF computed using weight functions presented a mean relative difference between straight and kink paths of less than 8% for 20° and less than 4% for 15° for crack lengths of the order of 150 μm. This difference is even less when the FE models using the J-integral are analyzed: in this case, the mean relative differences are about 2% for both angles. Thus, the simplification used in this work for the crack path seems reasonable. Moreover, for the straight crack, the average relative difference between the stress intensity factors calculated with the FE model using J-integral and the ones obtained using weight function is 2.29%.

The results show no significant discrepancy for different K_I values when the crack is perpendicular to free surface. This relative convergence of results probably occurs because as soon as the crack starts propagating in the next stage, it continues to grow perpendicularly to the direction of the maximum positive stress [33] and this path then coincides to the one hereby proposed. Thus, such match is even more expected in cases that the kinked portion of the crack is very small when compared to the overall length. Indeed, this agrees with what had been previously studied by [45], in which it was demonstrated for cracks with initial 45° kink angle that even for reasonably high b/c (Fig. 6) ratios, if the remote loading is a uniform tension parallel with the free surface of the specimen, the crack tips SIF will not differ much from the ones obtained for a straight crack.

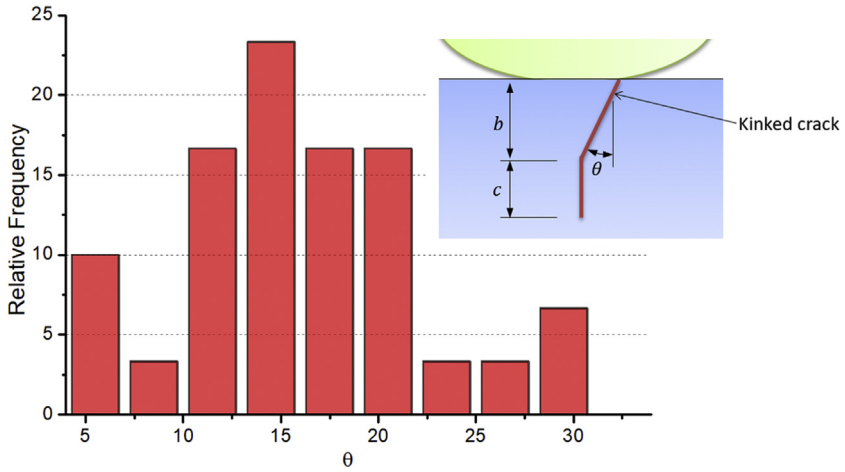

Fig. 6. Frequency of kink angles found in the literature and numerical model considering crack kink.

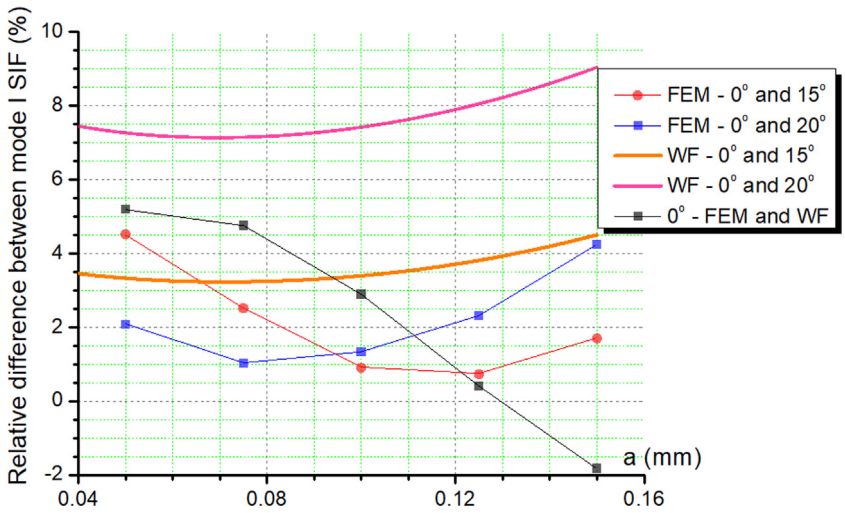

Fig. 7. Comparison between K_I obtained by FEM and weight functions.

The stress fields obtained in one of the FEM is illustrated in Fig. 8. They provide valuable information, as the magnitude of each stress component when the maximum bulk stress is reached.

All stress fields found in other simulations presented similar behavior. Therefore, their results will be omitted. The stress distribution along the crack path starting at the point with maximum value, $\sigma_{x(max)}$, on the surface of the specimen and the evolution of the maximum stress fields in each step are shown in Fig. 9.

It is evident from Fig. 9(b) that σ_x will be the most significant stress, forcing the crack to grow. When $\sigma_x = \sigma_{x_{max}}$, the σ_y/σ_x ratio is practically null, while $\tau_{xy}/\sigma_x \approx 15\%$. The present shear stress, albeit much smaller than the maximum normal stress, is of some significance. Therefore, the final question regarding the assumed conditions is how much has been neglected upon ignoring K_{II} in this work. To answer that question, Fig. 10 shows the difference between K_{eq} and K_I. Two K_{eq} were considered: (a) K_{eq} model based on the displacements behind the crack tip reaching a critical value, proposed by Tanaka [46] and (b) K_{eq} derived for elastic loading under plane stress conditions, based on the relations between the potential energy release rate G and the SIF [47]. These equations are presented, respectively, by:

$$K_{eq} = [K_I^4 + 8K_{II}^4]^{1/4} \text{and} K_{eq} = \sqrt{K_I^2 + K_{II}^2} \tag{7}$$

The first model gives a difference of less than 1.8% and the second one gives a difference of less than 4.5%. However, this difference is unrealistic, because when the mode II stress intensity factors present significant values, the crack tips tend to kink to minimize K_{II}, as it is seen in numerical simulations in compact tension and bending specimens and observed in fatigue experiments [48,49] with relative differences of less than 0.1 %.

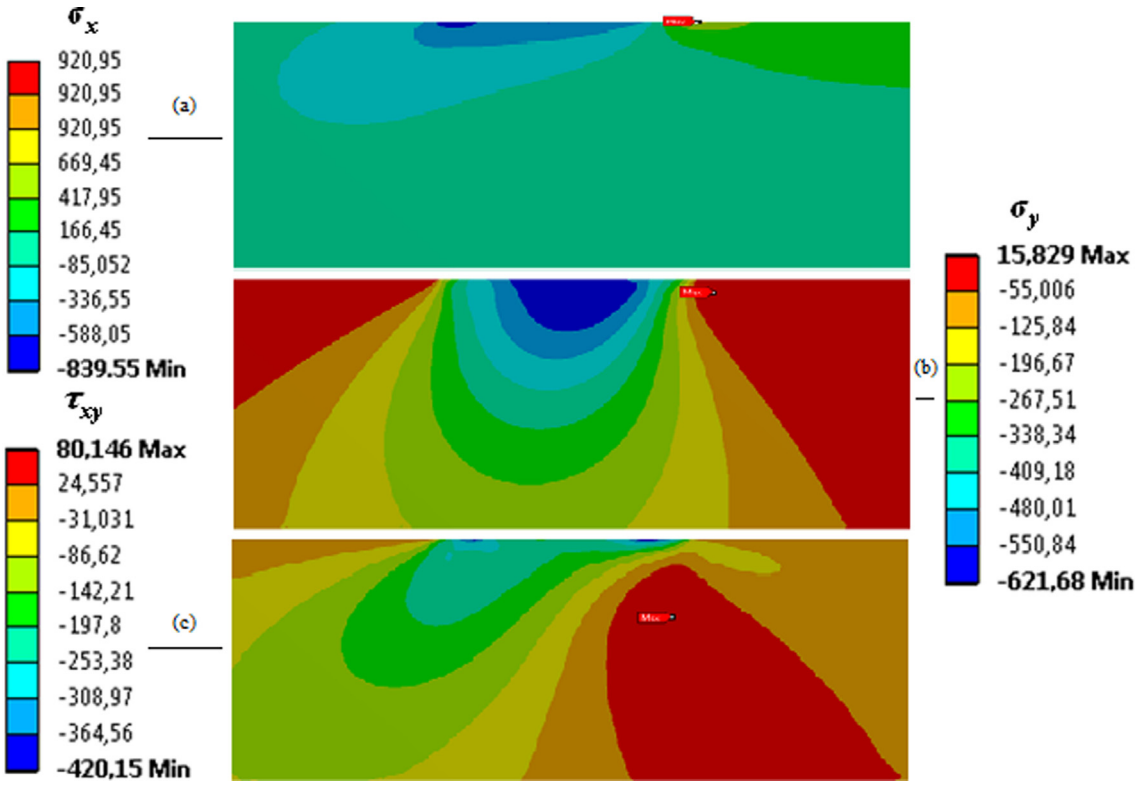

Fig. 8. (a)σ_x, (b)σ_y and (c) τ_{xy}, in MPa, for steel σ_b = 100 MPa and $\mu = 0.9$.

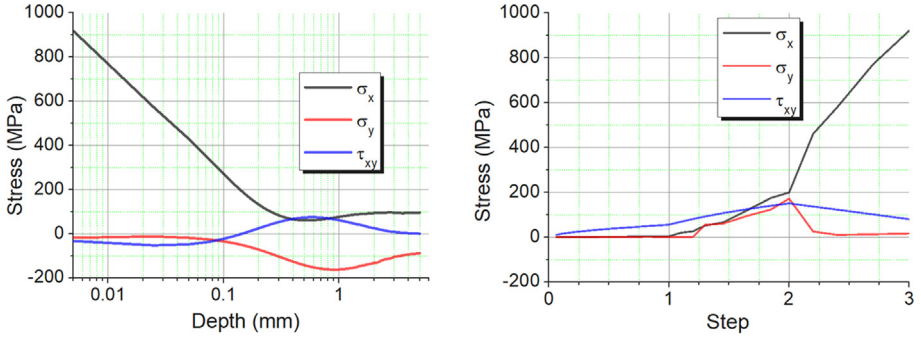

Fig. 9. Stress distribution along the chosen path (a) evolution of the maximum stress fields in each step (b) – steel σ_b = 100 MPa and $\mu = 0.9$.

5. Results and discussion

After validation, it was finally possible to compute $K_{gr}(a/w)$ using the equation:

$$K_{gr}(a/w) = \frac{K_{I(fretting)}}{K_{I(ref)}} \tag{8}$$

where $K_{gr}(a/w)$ is the Stress Gradient Factor, $K_{I(fretting)}$ is the SIF for fretting conditions, $K_{I(ref)}$ is a reference (TSIS specimen) SIF that depends on the applied bulk stress range, on the crack length a and on a geometric function $f(a/w)$.

As illustrated in Fig. 11, the smaller the COF, the smaller the initial K_{gr} values were. This can be explained because higher values of COF produce higher nominal stresses under the contact zone for the same applied bulk stress. This raises $K_{I(fretting)}$ for smaller crack lengths but not $K_{I(ref)}$. It can also be clearly seen in Fig. 11 the convergence of all K_{gr} curves. Johnson [50] states that the maximum depth z which is influenced by the contact pressure for a contact semi-width e is z = 0.78e, computed to be at approximately z = 0.44 mm (a/w = 0.044) for this model. In this case, the K_{gr} curves will converge for even

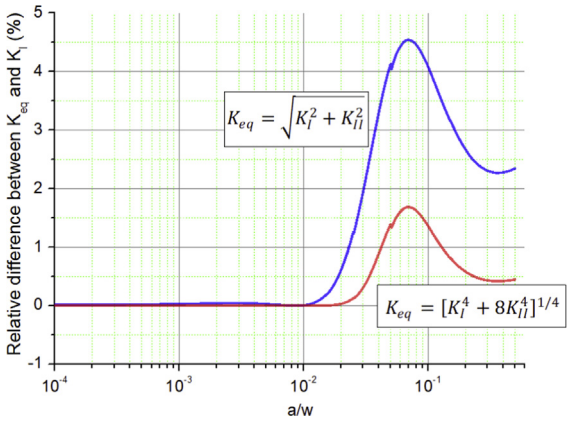

Fig. 10. SIF comparison upon neglecting K_{II}.

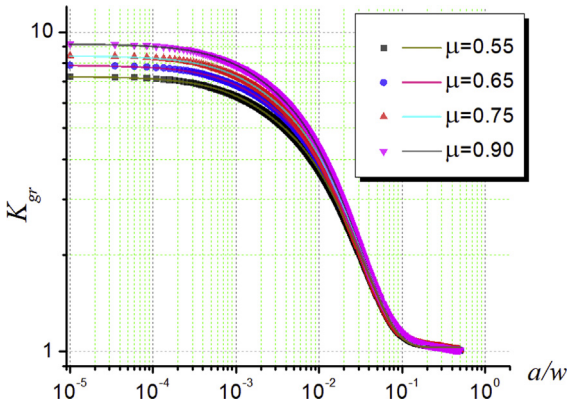

Fig. 11. Steel - K_{gr} curves and their respective fits for σ_b = 100 MPa varying the COF.

smaller crack lengths, a, because the stress increments caused by solely varying the COF was not that significant. In other words, changing the COF but maintaining the same bulk stress for the same material shows only appreciable K_{gr} differences for very small crack lengths. Finally, the curve fits presented in Fig. 11 show good point dispersion predictions and their equations are found in Appendix B. The displayed K_{gr} results obtained for steel followed the same behavior for all other tested materials.

Fig. 12 presents K_{gr} varying the bulk stress and considering fixed COF and material (steel). When the applied bulk stress is increased, K_{gr} is reduced for a/w $\leqslant$ 0.008, approximately. This occurs because raising the bulk stress causes the initial values of $K_{I(ref)}$ to be increased substantially more than the ones obtained for $K_{I(fretting)}$. The K_{gr} curves also present a change in their slope. In this fixed COF case, convergence of the different K_{gr} only occurs when the contact pressure exerts practically no influence on the crack growth. For σ_b = 80 MPa and 100 MPa, the curve fits can perfectly predict points dispersion. Although the curve fit forσ_b = 60 MPa has satisfactory results until a/w $\approx$ 0.03, longer cracks cannot be consistently fit into the proposed equation. However, for cracks longer than that, the K_{gr} curve fit values would return values lower than 1, which would not make any physical sense. Therefore, their equations were adjusted so that in this scenario, a stress gradient factor of 1 would be returned.

For fixed COF and applied bulk stress, the K_{gr} curves for the three different materials are presented in Fig. 13. The higher the modulus of elasticity of a material, the higher the K_{gr}values for the same crack length for small cracks (a/w $\approx$ 0.01, in this case). This occurs because considering the same geometry, the same load will result in a higher contact pressure for a higher modulus of elasticity. The higher contact pressure causes $K_{I(fretting)}$ values to be higher but does not alter $K_{I(ref)}$ significantly. Thus, materials with higher modulus of elasticity present higher K_{gr} values for small cracks but once the contact pressure stops exerting its influence, the opposite occurs. This happens because $K_{I(fretting)}$ values start decreasing significantly, as $K_{I(ref)}$ remains unaltered by the end of the contact pressure influence.

Finally, Fig. 14 illustrates the consequences of varying pad radii with all other parameters fixed. It demonstrates that smaller the pad radius is the higher K_{gr} becomes for the same crack length until a/w $\approx$ 0.01. This accords to the previous hypothesis that higher contact pressures cause $K_{I(fretting)}$ values to be higher but not significantly $K_{I(ref)}$, displaying higher

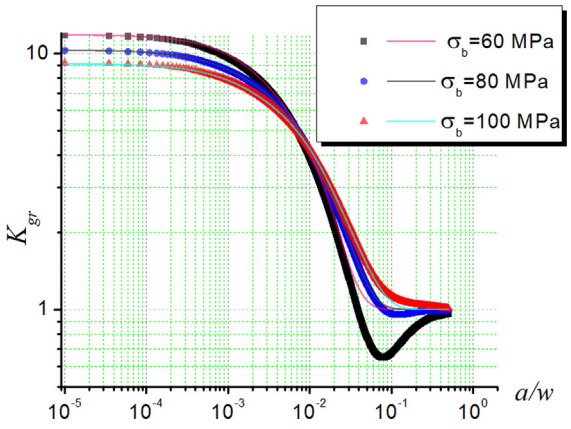

Fig. 12. Steel - K_{gr} curves and their respective fits for COF = 0.9 varying bulk stress.

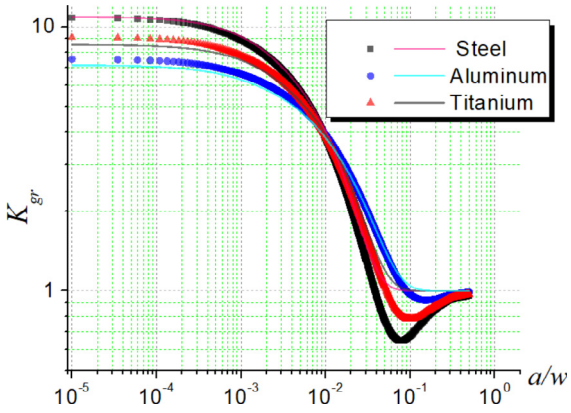

Fig. 13. Titanium, Steel and Aluminum - K_{gr} curves and their respective fits for COF = 0.75 and σ_b = 60 MPa.

K_{gr} initially. Naturally, smaller pads produce less contact area as well as higher contact pressures and for the same clamping force.

Interestingly, in all cases the different $K_{gr}(a/w)$ fit into equations of the same structure as (9), each with its own coefficients, which are presented in Appendix B.

$$K_{gr}(a/w) = A_1 e^{[(-a/w)/t_1]} + A_2 e^{[(-a/w)/t_2]} + A_3 e^{[(-a/w)/t_3]} + 1 \tag{9}$$

6. Applicability

The results hereby presented were computed for 2D models. Since real cracks propagate in 3D structures, it is necessary to treat them with a 3D correction factor, such as proposed by [6,51]. Navarro et al. [6] used a constant 3D correction factor of 0.78 for elliptical cracks. However, this correction factor is still far from realistic and can be improved using weight function results obtained by Vázquez et. al. [52], in which a linear correction is computed by:

$$3DFactor(a/w) = 0.55 + 1.27(a/w) \leqslant 1 \tag{10}$$

The results presented in this work are of comprehensive applicability and should be considered as general solutions as present by [22], for example. The authors suggest applying the presented SIF fretting solution for the following methods:

6.1. Strain-Based Fracture Mechanics (SBFM) [53,54]

Originally, K_{gr} was proposed to compute lives in components with notch root [25,55] and extended later to welded components [26,27,56]. In this case, even though the obtained K_{gr} already consider the presence of cracks along the extracted stress field, they are still limited to local elastic stresses. Under fretting, however, the plastic deformation in certain areas,

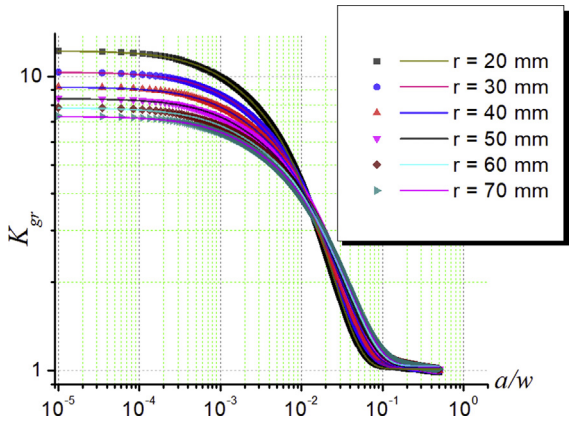

Fig. 14. Steel – K_{gr} curves for σ_b= 100 MPa and COF 0.75, varying pad radii.

especially in the contact region, may not be neglected. Therefore, it is necessary to use the SBFM, which unlike the linear elastic fracture mechanics, computes different SIF using deformations instead of stresses, given by:

$$\Delta K = E\Delta\varepsilon\sqrt{\mu a}\cdot f(a/w) \tag{11}$$

where ΔK is the stress intensity factor range, E is Young Modulus, $\Delta\varepsilon$ is the local inelastic strains when a hysteresis loop is created using Neuber's rule and Ramberg-Osgood material model to a determined applied nominal stress. The K_{gr} is used in Neuber's rule instead of K_t:

$$[K_{gr}(a/w)]^2 = \frac{\Delta\varepsilon\Delta\sigma}{\Delta\varepsilon_n\Delta\sigma_n} \tag{12}$$

where $\Delta\sigma\Delta\varepsilon$ are the local inelastic stress/stain and $\Delta\sigma_n\Delta\varepsilon_n$ is the nominal inelastic stress/strain.

6.2. Theory of Critical Distances (TCD) [57,58]

In the TCD, Taylor [59] assumes a characteristic material length parameter, the so-called critical distance L, previously defined by Haddad, Smith and Topper [53],which can be estimated from ΔK_R (long-crack SIF range threshold for a stress ratio R) and ΔS_R (smooth specimen fatigue limit at R ≠ 0):

$$L = \frac{1}{\pi}\left(\frac{\Delta K_R}{\Delta S_R}\right)^2 \tag{13}$$

In the analysis of uncracked notched components, the stress distribution is needed to determine the smooth specimen fatigue limit ΔS_R using the Point Method (PM) or Line Method (LM). For instance, the PM criterion for crack propagation (fatigue limit) is that the *local stress* at a distance x = L/2 ahead of the notch tip equals to the smooth specimen fatigue limit ΔS_R. This way, this criterion uses a relation among a *local stress* distribution, ΔS_R and L which does not make much sense with Eq. (13), which is a relationship among a SIF, ΔS_R and L.

Fig. 15 shows the difference between $\sigma_x(y)/\sigma_n$ (normalized local stress distribution) and K_{gr} for a typical FE model analyzed previously in section 5. It is possible to note a difference of approximately 200% between the curves when y = 0.5 (a/w = 0.1), for example. Therefore, the authors suggest applying K_{gr} curve in the TCD method instead of local stress distribution, $\sigma_x(y)$, because it creates a relationship among a SIF, ΔS_R and L which is more consistent with Eq. (13).

6.3. Stress gradient [60,61]

This model predicts the behavior of short cracks departing from notch tips provoked by fatigue. It computes the local stresses using a stress intensity factor for each point dependent of a function of both the crack size and the notch radius. That function tends to the classical K_t when the crack length is null and may be replaced by the correspondent K_{gr} curve in order to consider correct behavior of short cracks. The model also needs to derivate the stress/SIF gradient and, in the case of the fretting application herein proposed:

$$\frac{d[K_{gr}(a/w)]}{da} = -\frac{A_1 e^{[(-a/w)/t_1]}}{wt_1} - \frac{A_2 e^{[(-a/w)/t_2]}}{wt_2} - \frac{A_3 e^{[(-a/w)/t_3]}}{wt_3} \tag{14}$$

Additionally, the SIF solutions are a viable way to consider variable amplitude loading in fretting analysis. The solutions provided in this work can be properly adjusted by interpolating the K_{gr} curves. Furthermore, it is possible to develop them to become a broader equation containing amplitude variation parameters.

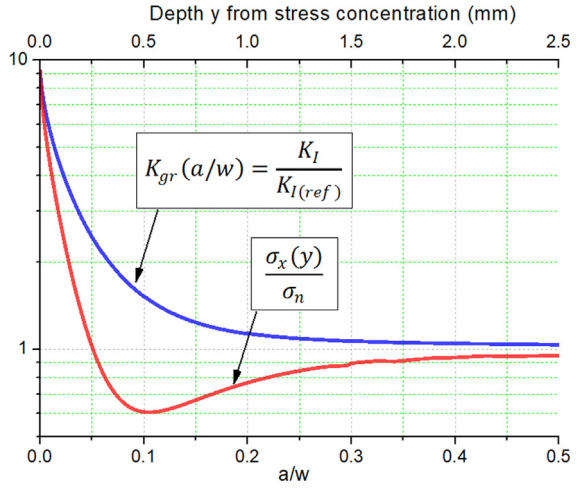

Fig. 15. Difference between K_{gr} and normalized local stress distribution.

4. Conclusions

In this work, a new approach to K_{gr} which can be used in fretting fatigue life estimation was presented. It was also demonstrated how important fretting fatigue parameters affect K_{gr}. Despite the complex nature of the fretting phenomenon, the K_{gr} curves demonstrated predictability and were, at least for most cases, perfectly fit into equations. Moreover, further development of the K_{gr} curves embracing amplitude variation parameters should make them an even more powerful tool for fretting analysis.

For the study of parameters that influence the value of K_{gr}, 41 models were produced. In the contact region, the higher COF and the modulus of elasticity, the higher the initial values of K_{gr}. The opposite happens when the normal tension and the pad radius increase, that is, the initial values of K_{gr} decrease. In general, the curves of K_{gr} have the same equation and converge to 1 as they move away from the contact region, as expected.

The numerical model proposed in this study considers the non-linear effects caused by the contact between pad and specimen. However, it is a 2D model using elastic material behavior. For real crack problems, a 3D correction factor must be introduced and may be used together with SBFM, for instance, in order to consider plastic behavior of materials. On the other hand, the SGF concept may be used to estimate the notch fatigue limit satisfactorily or even to predict the behavior of short cracks using the stress gradient method.

Albeit this study was limited to presenting solutions for bulk stress loading, it is possible to further expand the usefulness of K_{gr} to include bending loading as well, which can be relevant in some fretting situations. Moreover, future studies may include variable COF and a wear coefficient.

Finally, it is possible to produce a handbook of K_{gr} for different geometries and loading situations, as accomplished by Tada et al. [15] for different SIF, for example.

Appendix A. – Weight function coefficients for a single edge crack in a finite width [29]:

$$
\begin{aligned}
M_1 &= \frac{-0.029207 + \frac{a}{w}\left\{0.213074 + \frac{a}{w}\left[-3.029553 + \frac{a}{w}\left(5.901933 - \frac{a}{w}2.657820\right)\right]\right\}}{1.0 + \frac{a}{w}\left(-1.259723 + \frac{a}{w}\left\{-0.048475 + \frac{a}{w}\left[0.481250 - \frac{a}{w}\left(-0.526796 + \frac{a}{w}0.345012\right)\right]\right\}\right)} \\
M_2 &= \frac{0.451116 + \frac{a}{w}\left\{3.462425 + \frac{a}{w}\left[-1.078459 + \frac{a}{w}\left(3.558573 - \frac{a}{w}7.553533\right)\right]\right\}}{1.0 + \frac{a}{w}\left(-1.496612 + \frac{a}{w}\left\{0.764586 + \frac{a}{w}\left[-0.659316 - \frac{a}{w}\left(0.258506 + \frac{a}{w}0.114568\right)\right]\right\}\right)} \\
M_3 &= \frac{0.427195 + \frac{a}{w}\left\{-3.730114 + \frac{a}{w}\left[16.276333 + \frac{a}{w}\left(-18.799956 + \frac{a}{w}14.112118\right)\right]\right\}}{1.0 + \frac{a}{w}\left(-1.129189 + \frac{a}{w}\left\{0.033758 + \frac{a}{w}\left[0.192114 + \frac{a}{w}\left(-0.658242 + \frac{a}{w}0.554666\right)\right]\right\}\right)}
\end{aligned}
\tag{15}
$$

Appendix B. – K_{gr} fit equations

The following equations were adjusted using the commercial software ORIGIN with non-linear curve fittings using the inbuilt ExpDec3function.

$$K_{gr}(a/w) = A_1 e^{[(-a/w)/t_1]} + A_2 e^{[(-a/w)/t_2]} + A_3 e^{[(-a/w)/t_3]} + 1 \tag{16}$$

Tables B1–B4

Table B.1
- K_{gr} for steel.

σ_{bulk}	PARAMETER	COF			
		0.55	0.65	0.75	0.90
60 MPa	A_1	3.45558	2.31799	3.67544	3.15418
	t_1	0.01182	0.00169	0.01132	0.00186
	A_2	2.97827	3.3582	3.6241	2.50623
	t_2	0.01182	0.01154	0.01131	0.01108
	A_3	2.05065	3.56465	2.62644	5.19824
	t_3	0.00164	0.01154	0.00176	0.01108
80 MPa	A_1	1.78104	2.0354	5.01582	2.93337
	t_1	0.00403	0.00435	0.01696	0.00478
	A_2	0.84247	4.84487	2.36391	1.25324
	t_2	8.53702E-4	0.01713	0.00459	9.00113E-4
	A_3	4.56288	0.9805	1.10245	5.14449
	t_3	0.01741	8.9171E−4	9.03226E−4	0.01684
100 MPa	A_1	3.04794	3.11785	2.95865	1.38952
	t_1	0.02666	0.02682	0.00819	0.00127
	A_2	2.12894	2.54259	3.15796	3.53281
	t_2	0.00746	0.00802	0.02678	0.00808
	A_3	1.04404	1.17054	1.2683	3.2154
	t_3	0.00127	0.00131	0.0013	0.02664

Table B.2
K_{gr} for aluminum.

σ_{bulk}	PARAMETER	COF			
		0.55	0.65	0.75	0.90
60 MPa	A_1	4.36107	4.20847	1.45383	1.28087
	t_1	0.02166	0.02234	0.00502	0.00454
	A_2	2.06476	1.66238	0.65739	0.56646
	t_2	0.00553	0.00536	9.65E−04	8.94E−04
	A_3	0.78989	0.72815	4.0507	3.82767
	t_3	0.00108	9.98E−04	0.02255	0.02267
80 MPa	A_1	2.12661	0.77418	0.77418	1.52008
	t_1	0.0088	0.00139	0.00139	0.00829
	A_2	0.86358	1.75216	1.75216	2.83924
	t_2	0.00137	0.00861	0.00861	0.0321
	A_3	3.03016	2.9401	2.9401	0.70446
	t_3	0.03156	0.03181	0.03181	0.00139
100 MPa	A_1	2.23321	2.15243	2.11648	1.35534
	t_1	0.04359	0.04421	0.04384	0.01132
	A_2	2.14789	0.7498	0.6744	0.60815
	t_2	0.01206	0.00187	0.00184	0.00186
	A_3	0.83533	1.80042	1.5351	1.95588
	t_3	0.0018	0.01213	0.01155	0.04519

Table B.3
K_{gr} for titanium.

σ_{bulk}	PARAMETER	COF			
		0.55	0.65	0.75	0.90
60 MPa	A_1	2.39166	2.18723	2.81259	1.77328
	t_1	0.00343	0.00224	0.01507	0.00204
	A_2	5.8945	2.99415	2.81271	2.72187
	t_2	0.01486	0.01454	0.01507	0.01543
	A_3	0.82885	2.93809	1.93458	2.49846
	t_3	7.13804E−4	0.01454	0.00211	0.01543
80 MPa	A_1	2.51461	2.0404	3.81197	3.57289
	t_1	0.00631	0.00611	0.02223	0.02265
	A_2	4.03025	0.95274	1.74468	1.52793
	t_2	0.02199	0.0011	0.00577	0.00547
	A_3	1.07097	3.92722	0.85068	0.7497
	t_3	0.00109	0.02213	0.00109	0.00106

Table B.3 (*continued*)

σ_{bulk}	PARAMETER	COF			
		0.55	0.65	0.75	0.90
100 MPa	A_1	1.05884	2.30723	0.89272	1.97717
	t_1	0.00144	0.00954	0.00144	0.00915
	A_2	2.76371	2.68424	1.97717	2.65228
	t_2	0.00956	0.03286	0.00915	0.03273
	A_3	2.73935	0.9693	2.65228	0.89272
	t_3	0.03269	0.00147	0.03273	0.00144

Table B.4
K_{gr} for steel - $\sigma_{bulk} = 100$ MPa and COF = 0.75.

PARAMETER	r (mm)					
	20	30	40	50	60	70
A_1	4.9114	3.74832	3.3405	2.95865	2.63522	2.49914
t_1	0.01593	0.00664	0.0076	0.00819	0.00864	0.00945
A_2	4.36714	1.63779	1.43242	3.15796	3.00311	1.04062
t_2	0.00542	0.00113	0.00124	0.02678	0.02932	0.00146
A_3	1.94421	3.94756	3.41195	1.2683	1.14545	2.73988
t_3	0.00102	0.02032	0.02407	0.0013	0.00126	0.03216

References

[1] Madge JJ, Leen SB, McColl IR, Shipway PH. Contact-evolution based prediction of fretting fatigue life: effect of slip amplitude. Wear 2007;262:1159–70.
[2] Kim HS, Mall S, Ghoshal A. Two-dimensional and three-dimensional finite element analysis of finite contact width on fretting fatigue. Mater Trans 2011;52:147–54.
[3] Nowell D, Hills DA. Mechanics of fretting fatigue tests. Int J Mech Sci 1987;29:355–65.
[4] Talemi RH, Wahab MA, Baets PD. Numerical modelling of fretting fatigue. J Phys: Conf Ser 2011;305:012061.
[5] Baietto MC, Pierres E, Gravouil A, Berthel B, Fouvry S, Trolle B. Fretting fatigue crack growth simulation based on a combined experimental and XFEM strategy. Int J Fatigue 2013;47:31–43.
[6] Navarro C, García M, Domínguez J. A procedure for estimating the total life in fretting fatigue. Fatigue Fract Eng Mater Struct 2003;26:459–68.
[7] Luke M, Burdack M, Moroz S, Varfolomeev I. Experimental and numerical study on crack initiation under fretting fatigue loading. Int J Fatigue 2016;86:24–33.
[8] Nigro C, Sun L, Meriaux J, Proudhon H. Microstructural simulations of the initiation and propagation of short fretting cracks in a Ti–6Al–4V contact. Tribol Int 2014;74:103–9.
[9] Rammohan YS, Murthy H. Three dimensional finite element analysis of partial slip contacts subjected to combined loading. Finite Elem Anal Des 2012;56:9–19.
[10] Liu J, Shen HM, Yang YR. Finite element implementation of a varied friction model applied to torsional fretting wear. Wear 2014;314:220–7.
[11] Pierres E, Baietto MC, Gravouil A, Morales-Espejel G. 3D two scale X-FEM crack model with interfacial frictional contact: application to fretting fatigue. Tribol Int 2010;43:1831–41.
[12] Lévesque F, Goudreau S, Cloutier L, Cardou A. Finite element model of the contact between a vibrating conductor and a suspension clamp. Tribol Int 2011;44:1014–23.
[13] Giner E, Navarro C, Sabsabi M, Tur M, Domínguez J, Fuenmayor FJ. Fretting fatigue life prediction using the extended finite element method. Int J Mech Sci 2011;53:217–25.
[14] Bartha BB, Nicholas T, Farris TN. Modeling of geometry effects in fretting fatigue. Tribol Int 2006;39:1131–41.
[15] Gandiolle C, Fouvry S. Experimental analysis and modeling of the crack arrest condition under severe plastic fretting fatigue conditions. Proc Eng 2013;66:783–92.
[16] Proudhon H, Basseville S. Finite element analysis of fretting crack propagation. Eng Fract Mech 2011;78:685–94.
[17] Ding J, Kang G, Zhu Y, Zhu M. Finite element analysis on bending fretting fatigue of 316L stainless steel considering ratchetting and cyclic hardening. Int J Mech Sci 2014;86:26–33.
[18] Hills DA, Nowell D. Mechanics of Fretting Fatigue: Springer, Netherlands, 1994.
[19] Hills DA, Comninou M. An analysis of fretting fatigue cracks during loading phase. Int J Solids Struct 1985;21:721–30.
[20] Giummarra C, Brockenbrough JR. Fretting fatigue analysis using a fracture mechanics based small crack growth prediction method. Tribol Int 2006;39:1166–71.
[21] Ciavarella M, Berto F. A simplified extension of the Crack Analogue model for fretting fatigue with varying normal load. Theoret Appl Fract Mech 2017;91:37–43.
[22] Tada H, Paris PC, Irwin GR. The Stress Analysis of Cracks Handbook. ASME Press; 2000.
[23] El Haddad MH, Topper TH, Topper TN. Fatigue life predictions of smooth and notched specimens based on fracture mechanics. J Eng Mater Technol 1981;103:91–6.
[24] Dabayeh AA, Xu RX, Du BP, Topper TH. Fatigue of cast aluminium alloys under constant and variable-amplitude loading. Int J Fatigue 1996;18:95–104.
[25] Dabayeh AA, Berube AJ, Topper TH. An experimental study of the effect of a flaw at a notch root on the fatigue life of cast Al 319. Int J Fatigue 1998;20:517–30.
[26] Ghahremani K, Walbridge S. Fatigue testing and analysis of peened highway bridge welds under in-service variable amplitude loading conditions. Int J Fatigue 2011;33:300–12.
[27] Ghahremani K, Walbridge S, Topper T. A methodology for variable amplitude fatigue analysis of HFMI treated welds based on fracture mechanics and small-scale experiments. Eng Fract Mech 2016;163:348–65.
[28] Ingraffea AR. Computational Fracture Mechanics. In: Encyclopedia of Computational Mechanics, ed: John Wiley & Sons Ltd, 2004.
[29] Rice JR. Some remarks on elastic crack-tip stress fields. Int J Solids Struct 1972;8:751–8.
[30] Bueckner HF. A novel principle for the computation of stress intensity factors. ZAMM, 1970;vol. 50:p. 529–45.

[31] Wu XR, Carlsson J. Weight functions and stress intensity factor solutions. Pergamon Press; 1991.
[32] Fett T, Munz D. Stress intensity factors and weight functions. Computational Mechanics Publications; 1997.
[33] Glinka G, Shen G. Universal features of weight functions for cracks in mode I. Eng Fract Mech 1991;40:1135–46.
[34] Glinka G, Reinhardt W. Calculation of stress intensity factors for cracks of complex geometry and subjected to arbitrary nonlinear stress fields. In: STP1389, ASTM, 2000, p. 348–70.
[35] Chattopadhyay A, Glinka G, El-Zein M, Qian J, Formas R. Stress analysis and fatigue of welded structures. Welding in the World 2011;55:2–21.
[36] Namjoshi SA, Mall S, Jain VK, Jin O. Fretting fatigue crack initiation mechanism in Ti–6Al–4V. Fatigue Fract Eng Mater Struct 2002;25:955–64.
[37] Szolwinski MP, Farris TN. Observation, analysis and prediction of fretting fatigue in 2024–T351 aluminum alloy. Wear, 1998;vol. 221: p. 24–36.
[38] de Pannemaecker A, Fouvry S, Buffiere J-Y. Introduction of a reverse simulation approach to identify the fatigue stress intensity factor crack arrest threshold from fretting cracking experiments. Tribol Int 2014;76:122–32.
[39] de Pannemaecker A, Fouvry S, Buffiere JY. Reverse identification of short–long crack threshold fatigue stress intensity factors from plain fretting crack arrest analysis. Eng Fract Mech 2015;134:267–85.
[40] de Pannemaecker A, Fouvry S, Brochu M, Buffiere JY. Identification of the fatigue stress intensity factor threshold for different load ratios R: From fretting fatigue to C(T) fatigue experiments. Int J Fatigue 2016;82:211–25.
[41] de Pannemaecker A, Buffiere JY, Fouvry S, Graton O. In situ fretting fatigue crack propagation analysis using synchrotron X-ray radiography. Int J Fatigue 2017;97:56–69.
[42] Peng JF, Zhu MH, Cai ZB, Liu JH, Zuo KC, Song C, et al. On the damage mechanisms of bending fretting fatigue. Tribol Int 2014;76:133–41.
[43] Asai K. Fretting fatigue strength of 12% Cr steel under high local contact pressure and its fracture mechanics analysis. Proc Eng 2010;2:475–84.
[44] Kim H-K, Lee S-B. Crack initiation and growth behaviour of Al 2024–T4 under fretting fatigue. Int J Fatigue 1997;19:243–51.
[45] Hills DA, Kelly PA, Dai DN, Korsunsky AM. Solution of Crack Problems: The Distributed Dislocation Technique: Springer, Netherlands, 2013.
[46] Tanaka K. Fatigue crack propagation from a crack inclined to the cyclic tensile axis. Eng Fract Mech 1974;6:493–507.
[47] Irwin GR. Analysis of stresses and strains near the end of a crack traversing a plate. J Appl Mech 1957;24:361–4.
[48] de Oliveira Miranda AC, Meggiolaro MA, de Castro JTP, Martha LF. Fatigue life prediction of complex 2D components under mixed-mode variable amplitude loading. Int J Fatigue 2003;25:1157–67.
[49] Miranda ACO, Meggiolaro MA, Castro JTP, Martha LF, Bittencourt TN. Fatigue life and crack path predictions in generic 2D structural components. Eng Fract Mech 2003;70:1259–79.
[50] Johnson KL, Johnson KL. Contact Mechanics: Cambridge University Press, 1987.
[51] Newman I, Raju I. Stress Intensity Factor Equations for Cracks in Three-Dimensional Finite Bodies Subjected to Tension and Bending Loads - NASA Techcnical Memorandum 86793. In: NASA Techcnical Memorandum 86793 vol. 85, NASA, 1984.
[52] Vázquez J, Navarro C, Domínguez J. Two dimensional versus three dimensional modelling in fretting fatigue life prediction. J Strain Anal Eng Des 2016;51:109–17.
[53] El Haddad MH, Smith KN, Topper TH. Fatigue crack propagation of short cracks. J Eng Mater Technol 1979;101:42–6.
[54] El Haddad MH, Smith KN, Topper TH. STP677 - A Strain Based Intensity Factor Solution for Short Fatigue Cracks Initiating from Notches. In: Fracture Mechanics: Proceedings of the Eleventh National Symposium on Fracture Mechanics: Part I, ed: ASTM, 1979, p. 274–89.
[55] Khalil M, Topper TH. Prediction and correlation of the average crack-opening stress with service load cycles. Int J Fatigue 2003;25:661–70.
[56] Tehrani Yekta R, Ghahremani K, Walbridge S. Effect of quality control parameter variations on the fatigue performance of ultrasonic impact treated welds. Int J Fatigue 2013;55:245–56.
[57] Araújo JA, Nowell D. Analysis of pad size effects in fretting fatigue using short crack arrest methodologies. Int J Fatigue 1999;21:947–56.
[58] da Silva BL, Ferreira JLA, Araújo JA. Influence of notch geometry on the estimation of the stress intensity factor threshold by considering the Theory of Critical Distances. Int J Fatigue 2012;42:258–70.
[59] Taylor D. Geometrical effects in fatigue: a unifying theoretical model. Int J Fatigue 1999;21:413–20.
[60] Meggiolaro MA, Miranda ACdO, de Castro JTP. Short crack threshold estimates to predict notch sensitivity factors in fatigue. Int J Fatigue 2007;29:2022–31.
[61] de Castro JTP, Landim RV, Leite JCC, Meggiolaro MA. Prediction of notch sensitivity effects in fatigue and in environmentally assisted cracking. Fatigue Fract Eng Mater Struct 2015;38:161–79.